Monodisperse hematite porous nanospheres: synthesis, characterization, and applications for gas sensors

2008 Nanotechnology 19 125606

(http://iopscience.iop.org/0957-4484/19/12/125606)

Nanotechnology **19** (2008) 125606 (7pp) doi:10.1088/0957-4484/19/12/125606

Monodisperse hematite porous nanospheres: synthesis, characterization, and applications for gas sensors

Xinglong Gou[1,2], Guoxiu Wang[1], Jinsoo Park[1], Hao Liu[1] and Juan Yang[1]

[1] School of Mechanical, Materials and Mechatronic Engineering, University of Wollongong, Wollongong, NSW 2522, Australia
[2] School of Chemistry and Chemical Engineering, China West Normal University, Nanchong 637002, People's Republic of China

E-mail: gwang@uow.edu.au

Received 19 November 2007, in final form 21 January 2008
Published 21 February 2008
Online at stacks.iop.org/Nano/19/125606

Abstract

Monodisperse α-Fe_2O_3 porous nanospheres with uniform shape and size have been synthesized via a facile template-free route. X-ray diffraction (XRD), scanning electron microscopy (SEM), transmission electron microscopy (TEM), high-resolution TEM (HRTEM), and Raman spectroscopy were employed to characterize the product, showing the high quality of the as-prepared α-Fe_2O_3 porous nanospheres. Furthermore, the α-Fe_2O_3 porous nanospheres can selectively detect ethanol, formaldehyde and acetic acid, with a rapid response and high sensitivity, from a series of flammable and toxic/corrosive gases, indicating their potential applications for high sensitivity gas sensors.

1. Introduction

Chemical sensors play a very important role in both environmental protection and human health. The fabrication of metal oxide semiconducting nanomaterials with large surface-to-volume ratios for gas sensor applications is currently a major focus of nanoscience and nanotechnology [1–5].

As an important n-type semiconductor, hematite (α-Fe_2O_3) features non-toxicity, low cost, high stability, and environmental compatibility. It has been intensively investigated, due to its potential applications in gas sensors, rechargeable lithium-ion batteries, catalysts, pigments, magnetic devices, photoanodes for efficient water splitting by sunlight, waste-water treatment, and in other biological and medical fields [6–11]. For these applications much effort has been made to prepare nanostructured α-Fe_2O_3 with various morphologies [12–14]. From the viewpoint of gas sensor application, nanostructures with porous walls or hollow cavities are particularly desirable for improved sensing performance [15, 16]. To prepare α-Fe_2O_3 porous or hollow nanostructures, hard templates, such as porous alumina membranes [6], carbon nanotubes [7], and porous silica [17], or surfactants (sometimes called soft templates) [18] are usually involved. Recently, Suslick *et al* [19] produced an iron/carbon composite by first using ultrasound to irradiate a mixture of carbon nanoparticles and iron pentacarbonyl in hexadecane, and then obtained hollow hematite nanoparticles by elaborately controlling the oxidation of the resulting composite. Xu and co-workers [20] prepared α-Fe_2O_3 hollow nanospheres by controlled precipitation of Fe^{3+} with urea in the presence of carbonaceous saccharide nanospheres as hard templates. However, the template-direct synthesis suffers from the disadvantages of low yield and high cost. As an alternative route, template-free solution-based synthetic methods have also been reported as preparation methods for porous α-Fe_2O_3 nanostructures [13, 21, 22], such as nanotubes, nanorings, and porous nanorods. In this case, the presence of some inorganic salts, such as $NH_4H_2PO_4$, Na_2SO_4, Na_2SO_3, NH_4Cl, KCl, etc, is a prerequisite. In addition, the sorts and amounts of additives, as well as other experimental parameters, must be carefully selected and controlled. Therefore, it still remains a challenge to develop a facile template-free approach to synthesize α-Fe_2O_3 porous or hollow nanostructures with high gas sensing performance.

Herein, we report the synthesis of monodisperse α-Fe_2O_3 porous nanospheres with uniform shape and size, and their gas sensing properties towards a series of gases including

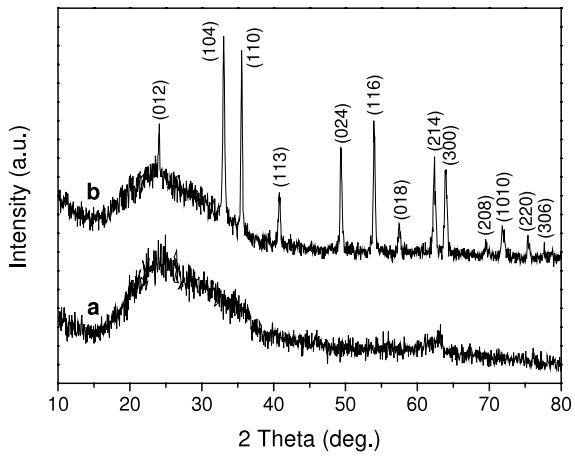

Figure 1. XRD patterns of the precursor (a) and the final product (b) after calcination treatment of the precursor.

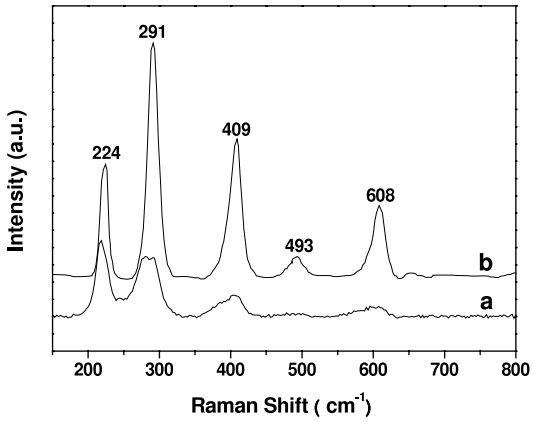

Figure 2. Raman spectra of the precursor (a) and the calcined product (b).

ethanol, acetone, heptane, gasoline, toluene, formaldehyde, acetic acid, and ammonia. The results show that the as-prepared α-Fe_2O_3 porous nanospheres can selectively detect ethanol, with a rapid response and high sensitivity, from other flammable and explosive gases, such as acetone, gasoline, toluene, and heptane. Furthermore, the as-prepared α-Fe_2O_3 porous nanospheres exhibit excellent sensing performance towards formaldehyde at low concentrations.

2. Experimental details

All of the chemicals, such as ferric nitrate, sodium citrate, and urea, are analytical grade and were used directly as purchased from Sigma-Aldrich. Hematite porous nanospheres of uniform size and shape were synthesized via a two-step process including hydrothermal synthesis of the precursor and a subsequent calcination treatment. In a typical procedure, 1 mmol $Fe(NO_3)_3{\cdot}9H_2O$, 2 mmol sodium citrate, and 2.5 mmol urea were sequentially dissolved in 15 ml de-ionized water under continuous stirring. The resulting transparent yellow-green solution was sealed into a Teflon-lined stainless steel autoclave of 25 ml capacity and heated at 160 °C for 10 h. After it cooled to room temperature naturally, a brown-yellow precipitate was collected, washed several times with de-ionized water and absolute ethanol, and dried in air at 60 °C for 4 h to obtain the precursor. The final red Fe_2O_3 powder was prepared by heating the previous precursor in air at 500 °C for 2 h.

The crystal structure and phase of the final products were determined by XRD using a Philips 1730 X-ray powder diffractometer with Cu Kα radiation. The morphology and microstructures of the hematite sample were characterized by a JEOL 6460 scanning electron microscope, by a JEOL 2011 transmission electron microscope, and by high-resolution TEM (HRTEM) coupled with energy-dispersive x-ray spectroscopy (EDS). Raman spectra were recorded on a Jobin-Yvon Horiba Micro Raman spectrometer model HR 800 with an excitation wavelength of 632 nm. Gas sensing measurements were carried out by a computer controlled WS-30A system.

3. Results and discussion

Figure 1 shows the XRD patterns of the hydrothermally synthesized precursor (a) and the final product (b) prepared after calcination treatment of the precursor. It can be seen that the precursor is x-ray amorphous in essence, and no certain crystallographic phase can be resolved. However, calcination treatment of the precursor not only changed the color of the powder from brown-yellow to red, but also remarkably improved its crystallinity. All of the diffraction peaks in pattern (b) can be easily indexed to pure rhombohedral phase of α-Fe_2O_3 (ICDD-JCPDS card No. 33-0664, a = 5.0356 Å, c = 13.7489 Å). No impurity phases were detected by XRD analysis, indicating that the amorphous precursor was completely transformed to crystalline hematite with high phase purity after the calcination treatment. The chemical composition of the products was further determined by EDS analyses (the data not shown here), which disclosed that both the precursor and the final product are only composed of O and Fe with the atomic ratio very close to the stoichiometric composition of Fe_2O_3.

Raman spectroscopy is an important tool to identify the crystal phase and determine the quality of crystalline or amorphous materials. The Raman spectra of both the precursor and the final product are presented in figures 2(a) and (b), respectively. On the whole, the spectra for the two samples are almost the same with the exception of peak intensity. There are five peaks at 224, 291, 409, 493, and 608 cm^{-1}, which can be respectively assigned to the A_{1g}, E_g, E_{1g}, A_{1g}, and E_g Raman modes for the typical hematite phase [23]. This result conforms that both the precursor and the calcined product are α-Fe_2O_3. No other iron oxides, such as magnetite or maghemite, were detected, indicating the high purity of the product. Compared to the reported values for the α-Fe_2O_3 dendritic architectures [24], all peaks of our products are slightly blue shifted. This may be caused by the small size of the component nanocrystals, which will be discussed below.

The general morphology of the as-prepared α-Fe_2O_3 product was observed by field emission SEM (FESEM), and typical images at different magnifications are shown in figure 3. Obviously, the hematite product is entirely

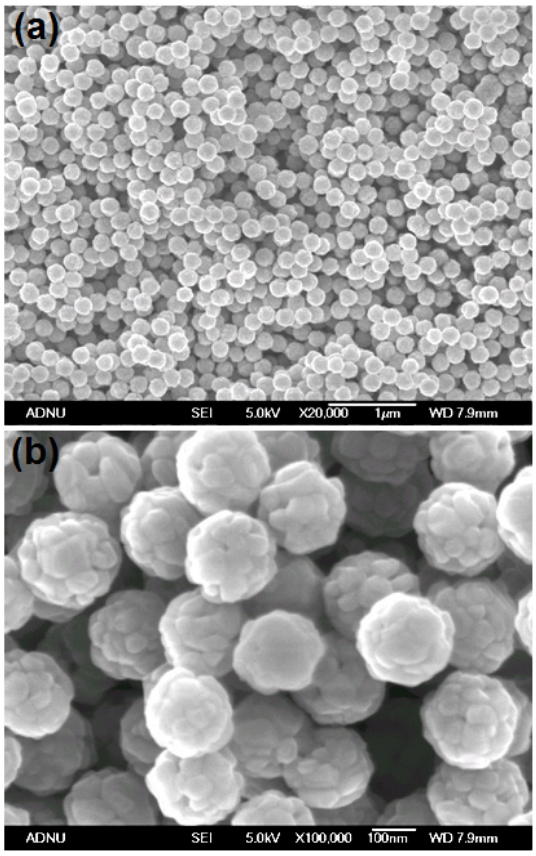

Figure 3. FESEM images of the as-prepared α-Fe_2O_3 product under different magnifications.

composed of uniformly dispersed nanospheres, as shown in figure 3(a). The spherical shape is very homogeneous, and the size of these nanospheres is about 180 nm, with a very narrow size distribution. Figure 3(b), which was taken under higher magnification, clearly reveals that the surface of the nanospheres consists of many small nanoparticles, and thus the surface is rough with a large amount of pores.

TEM and HRTEM can give further insight into the microstructure of the product. The low-resolution TEM image (figure 4(a)) confirms that spherical hematite nanostructures with uniform shape and a size of about 180 nm were produced, in good agreement with the SEM observation results. Meanwhile, the contrast in most of spheres suggests that these nanospheres may have a hollow cavity and a porous surface. The inset of figure 4(a) is the electron diffraction (ED) pattern taken from a large area, indicating the crystalline nature of the α-Fe_2O_3 product. Figures 4(b) and (c), taken under higher magnifications, reveal that these regular porous nanostructures are composed of many tiny nanoparticles, with sizes of 15–35 nm, which self-assemble into spheres, leading to the formation of numerous pores. The pore size in the nanospheres is less than 30 nm. Figure 4(d) shows an HRTEM image, which was taken from the framed part of a component nanoparticle. It displays regular lattice fringes with a spacing of 0.25 nm, corresponding to the lattice spacing (d-value) of the (110) planes of hematite. Furthermore, the HRTEM analysis, along with its corresponding fast Fourier transform (FFT) pattern (the inset) indicates that the component nanoparticles grew as single crystals of α-Fe_2O_3.

The formation mechanism of the porous α-Fe_2O_3 nanospheres is not clear at present, and it requires further

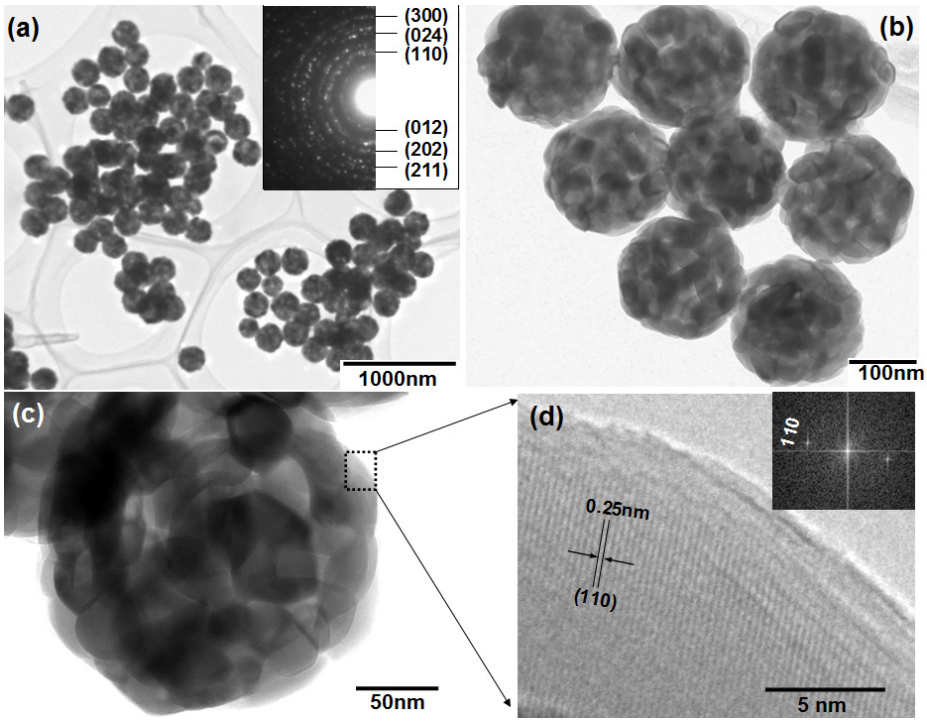

Figure 4. (a)–(c) TEM images of the as-prepared α-Fe_2O_3 product under different magnifications, with the inset of panel (a) an electron diffraction (ED) pattern taken from a large area; (d) HRTEM image taken from the framed part of a component nanocrystal in panel (c) along with its corresponding fast Fourier transform (FFT) image (the inset).

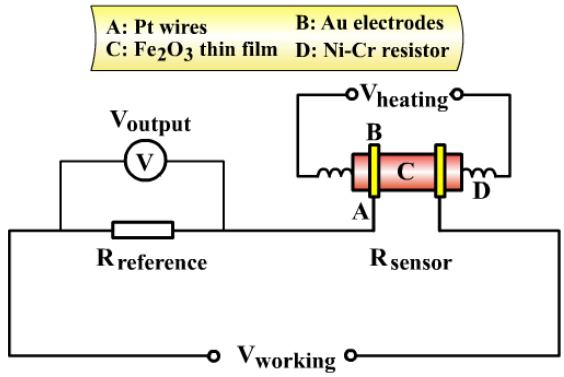

Figure 5. Schematic diagram of the gas sensor system. (This figure is in colour only in the electronic version)

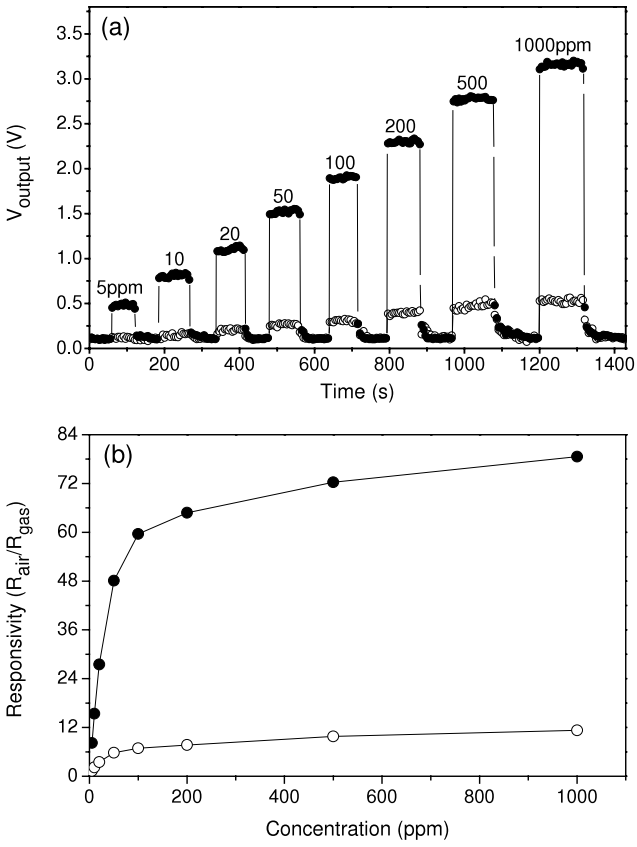

Figure 6. Ethanol sensing performance of the sensors based on the synthesized α-Fe_2O_3 nanospheres (solid dots) and on the commercial powder (hollow circles): (a) response curves on cycling between increasing concentrations of ethanol and ambient air; (b) responsivity as a function of ethanol concentration.

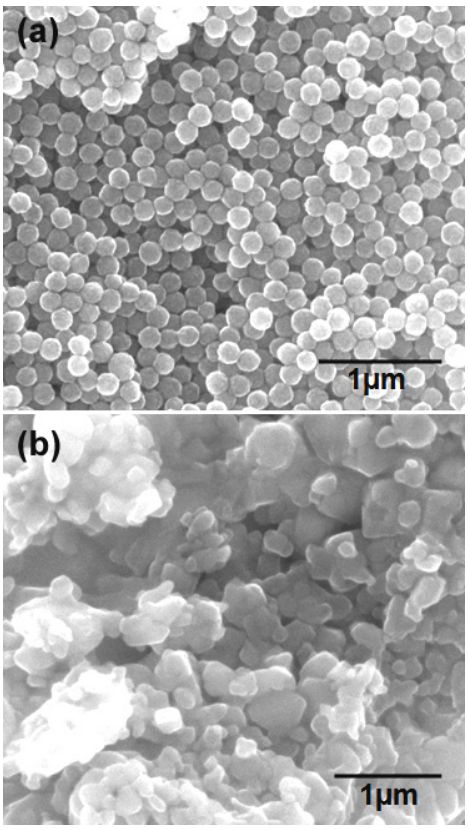

Figure 7. SEM images of the Fe_2O_3 films on the sensors based on the nanospheres (a) and the commercial powder (b).

investigations. However, the porous surfaces and hollow cavities of the monodisperse α-Fe_2O_3 nanospheres can facilitate gas molecule diffusion and the accompanying surface interaction. Furthermore, the unique stacking mode of monodisperse nanospheres can provide much more capacious interspaces than any other shapes. These features make the as-prepared α-Fe_2O_3 porous nanospheres a promising candidate for gas sensor applications. So we investigated the gas sensing performance of the α-Fe_2O_3 porous nanospheres. As a comparison, the sensing properties of the α-Fe_2O_3 commercial powder were also studied.

Figure 5 shows a schematic diagram of the sensor system. First, a mixture of the sample and alcohol was coated as a thin film on a ceramic tube with previously printed Au electrodes and Pt conducting wires. After heating at 400 °C in air for 2 h to evaporate the solvent and improve the stability of the device, a Ni–Cr resistor wire was crossed through the ceramic tube as a heater, allowing us to control the working temperature by adjusting the heating voltage ($V_{heating}$). Finally, a reference resistor was put in series with the sensor to form a complete measurement circuit. In the test process, the voltage (V_{output}) across the reference resistor changes with the sensor's resistance, which responds to the types and concentrations of the test gases. So, the response of the sensor in air or in a test gas can be measured by monitoring V_{output}. Our gas sensing measurements were carried out at a working temperature of 150 °C and 30% relative humidity (RH).

Figure 6(a) plots the real-time sensing response characteristics towards ethanol of the sensors based on the as-synthesized α-Fe_2O_3 nanospheres and on the commercial powder. Here, eight testing cycles were recorded, corresponding to eight different ethanol concentrations from 5 to 1000 ppm, respectively. It can be seen that V_{output} values increased abruptly upon the injection of ethanol and then decreased rapidly and recovered their initial value after the test gas was released. Moreover, the response magnitude of the α-Fe_2O_3 nanospheres

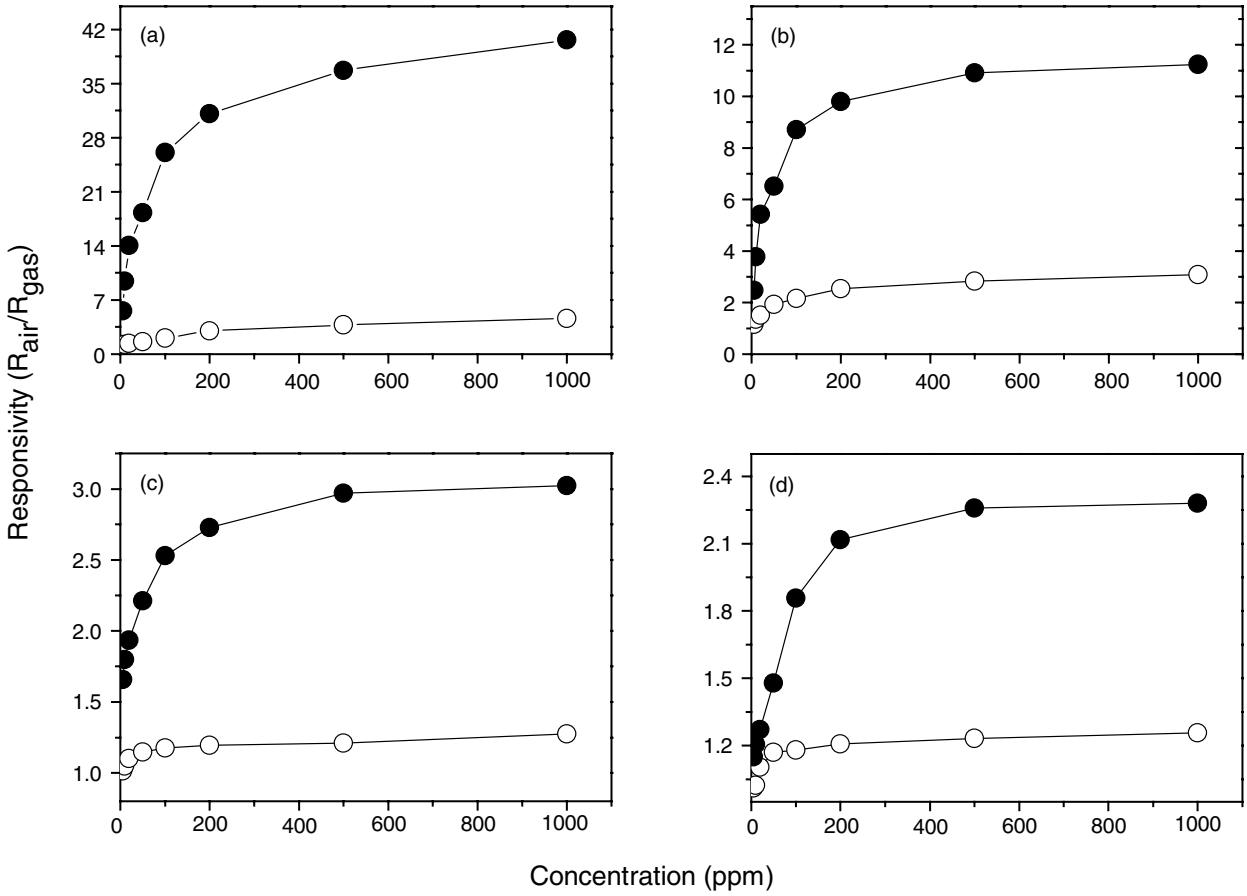

Figure 8. Responsivity of the sensors based on the as-prepared α-Fe_2O_3 nanostructures (solid dots) and on the commercial powder (hollow circles) as a function of the vapor concentration of some combustible gases: (a) acetone, (b) 92# gasoline, (c) heptane, (d) toluene.

improved dramatically with increasing concentration of the ethanol and was always higher than that of the commercial powder, suggesting that the Fe_2O_3 nanostructures are much more sensitive to ethanol than the commercial powder. The response times and recovery times (defined as the time required to reach 90% of the final equilibrium value) of the α-Fe_2O_3 nanospheres were less than 10 s, indicating their rapid respond and good reversibility.

From Ohm's law, the electric resistance of the α-Fe_2O_3 sensor accordingly underwent a decreasing and increasing process when the test gas (ethanol vapor) was turned on and off, respectively. The mechanism responsible for the gas sensing is considered to follow the surface conduction modulation [2, 11, 15]. α-Fe_2O_3 is an n-type semiconductor, in which the electrons are the majority carriers [11]. Its conductivity or electrical resistance can be changed by foreign gas molecules through tuning the carrier density. Reducing molecules such as ethanol will donate electrons to the α-Fe_2O_3 surface and thus decrease its resistance; the opposite holds true for oxidizing molecules. In clean air, oxygen molecules adsorb on the surface of the α-Fe_2O_3 thin film in the form of O_2^-, O^-, or O^{2-} by trapping free electrons from the surface, and increase the resistance of the α-Fe_2O_3 sensor. On exposure to ethanol vapor, ethanol molecules will absorb and react with the ionic oxygen species, and thus inject electrons to the α-Fe_2O_3 surface during the oxidation–reduction process, leading to a decrease in its resistance.

Responsivity, an important property of a gas sensor is defined as $S = R_{air}/R_{gas}$, where R_{air} and R_{gas} are the stationary electrical resistance of the sensor in air and in the test gas, respectively. Figure 6(b) shows the responsivities of the sensors based on the nanospheres and on the commercial powder as a function of ethanol vapor concentration. Generally, the responsivity of the α-Fe_2O_3 nanospheres is 5–8 times higher than that of the commercial powder. This result means that the ethanol sensing performance of the porous α-Fe_2O_3 nanospheres is much better than that of the commercial powder and is equivalent to that of polycrystalline nanotubes [6]. Meanwhile, it is worth noticing that the as-prepared nanospheres exhibit outstanding responsivity in low concentrations of ethanol atmosphere. For example, the responsivity of the nanosphere-based sensor exceeds 15 in 10 ppm of ethanol, and reaches 48 in 50 ppm of ethanol. This result suggests potential applications of these porous α-Fe_2O_3 nanospheres in biomedicine, food industries, and breath analyzers.

The improved sensing performance of the present porous α-Fe_2O_3 nanospheres may be attributed to their porous spherical structure. The numerous interconnected pores in the nanospheres can act as channels for diffusion of gas, and thus provide more active sites and improve the kinetics of

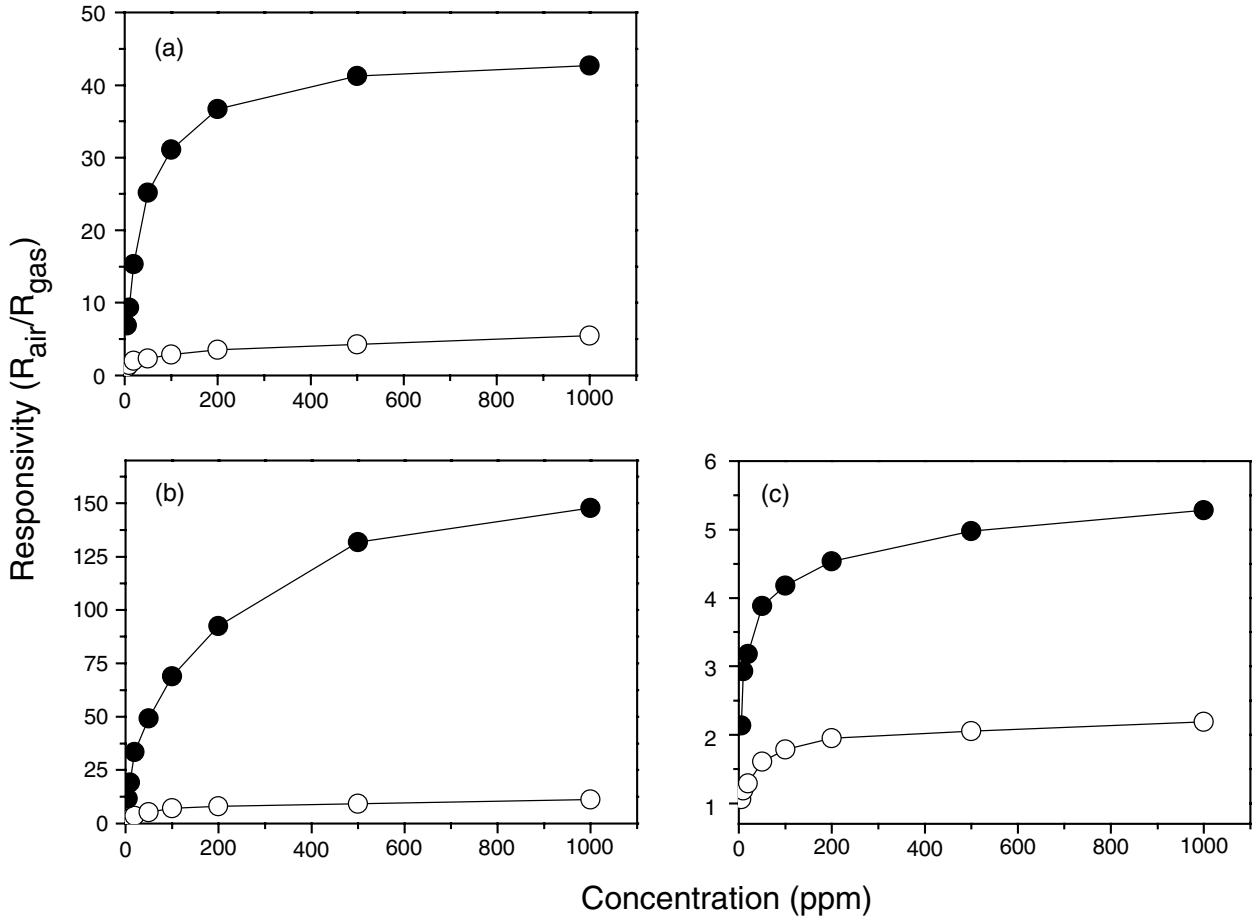

Figure 9. Responsivity of the sensors based on as-prepared α-Fe_2O_3 nanospheres (solid dots) and commercial powder (hollow circles) as a function of the vapor concentration of some toxic and corrosive gases: (a) formaldehyde, (b) acetic acid, (c) ammonia.

both the reaction of ethanol with surface-adsorbed oxygen and the replacement of the latter from the gas phase. On the other hand, the stacking of the monodisperse Fe_2O_3 nanospheres on the ceramic tube surface can further create much more capacious interspaces than any other shapes as shown in figure 7(a), resulting in sufficient space for the interaction between α-Fe_2O_3 and ethanol vapor. In contrast, the commercial powder is composed of solid particles with size in the range from 160 to 700 nm (figure 7(b)), which is much larger than the components of the nanospheres. Moreover, the commercial powders stacked into a more compact film on the ceramic tube surface, leading to smaller specific surface area and fewer active sites for the interaction with foreign gas molecules as that observed for the SnO_2 dense film produced by the chemical vapor deposition (CVD) approach [25]. Therefore, the commercial Fe_2O_3 powder exhibited much lower responsivity than the porous nanospheres.

Based on the successful measurement of ethanol sensing performance, we further investigated the sensing properties of the α-Fe_2O_3 sensors towards other flammable and explosive gases, such as acetone, 92# gasoline, heptane, and toluene. The corresponding results are shown in figures 8(a)–(d), respectively. It can be seen that the responsivities of the as-synthesized porous nanospheres were always much higher than that of the commercial powder, no matter what kind of gas was tested. From figure 8(a) one can see that the α-Fe_2O_3 nanospheres still exhibit high responsivity towards acetone, although the responsivity is lower than to ethanol. The responsivity towards gasoline (figure 8(b)) is much lower, due to the weak chemical interaction between gasoline and the α-Fe_2O_3 surface and the absorbed oxygen species at the relatively low working temperature. However, the sensor could barely detect heptane (figure 8(c)) and toluene (figure 8(d)) even when their actual concentrations were very high (for example 1000 ppm), because both heptane and toluene do not possess redox capability under usual conditions. These results illustrate that the sensor based on the porous α-Fe_2O_3 nanospheres has a certain degree of selectivity to flammable and explosive gases.

Air quality monitoring is another important application of metal oxide semiconducting sensors. So we investigated the sensing properties of the prepared α-Fe_2O_3 nanospheres to some toxic, corrosive, and irritating gases, such as formaldehyde (HCHO), acetic acid, and ammonia, and the measurement results are shown in figure 9. Similar to the detection of combustible gases, the sensing performance of the as-prepared nanospheres is much higher than that of the commercial powder. It is interesting that α-Fe_2O_3 nanospheres exhibited excellent sensing performance towards HCHO (figure 9(a)). The responsivity exceeded 9 in the presence of 10 ppm of HCHO, and it increased exponentially

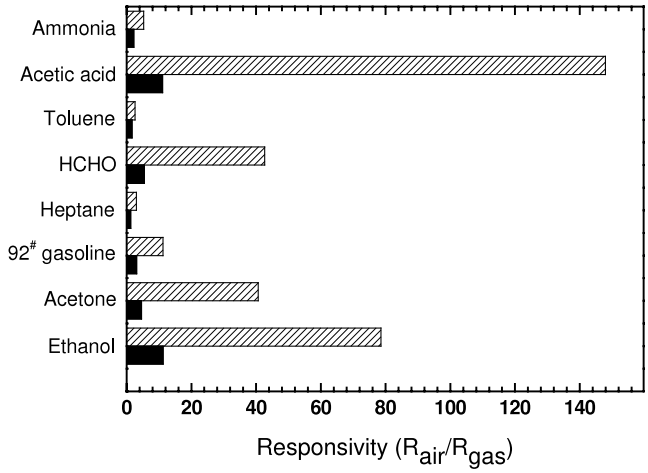

Figure 10. Responsivity of the sensors based on the as-prepared α-Fe_2O_3 nanospheres (slash) and on the commercial powder (black) towards different gases or vapors.

to 25 in 50 ppm of HCHO atmosphere. This result is much better than that reported for α-Fe_2O_3 nanorods [22], indicating the potential application of the porous α-Fe_2O_3 nanospheres in air quality monitoring in residential and office buildings.

It is interesting that the α-Fe_2O_3 nanospheres display high responsivity to acetic acid (figure 9(b)), which does not exhibit any distinct redox capability under usual conditions. The responsivity increased exponentially with increased gas concentration in the range 5–200 ppm, and reached 148 in the presence of 1000 ppm of acetic acid vapor. Here, the unusual high responsivity of the sensor to acetic acid may be caused by the strong chemiadsorption of acetic acid on the surface of the Fe_2O_3, due to the strong coordination of carboxyl to Fe^{3+} and the charge transfer transition from carboxyl to Fe^{3+} on the sensor surface. However, the α-Fe_2O_3 nanospheres seem not to be sensitive to ammonia (figure 9(c)).

For comparison, figure 10 presents the responsivity of the sensors based on the porous α-Fe_2O_3 nanospheres and on the commercial powder to eight types of gases or vapors at a concentration of 1000 ppm. It is obvious that the gas sensing performance of the α-Fe_2O_3 nanospheres was always better than that of the commercial powder, whichever gas was tested. At the given gas concentration, the α-Fe_2O_3 nanospheres showed the highest responsivity and selectivity towards acetic acid as opposed to any other gases. On the other hand, the α-Fe_2O_3 nanospheres can selectively detect ethanol in the presence of other flammable and explosive gases, such as acetone, gasoline, heptane, and toluene. In addition, the α-Fe_2O_3 nanospheres exhibited much higher responsivity towards formaldehyde than the reported value for porous α-Fe_2O_3 nanorods [22], indicating a potential application of the α-Fe_2O_3 porous nanospheres prepared by our method in detecting toxic gas.

The on and off responses could be repeated without perceptible changes in the signal after continuous measurement for three weeks or at regular intervals, illustrating its good reproducibility and long-term stability of the α-Fe_2O_3 nanosensor.

4. Conclusion

In summary, monodisperse α-Fe_2O_3 porous nanospheres of high quality have been successfully prepared via a two-step process, including hydrothermal synthesis of the precursor at low temperature and a subsequent thermal treatment. During the synthesis process, no hard template, surfactant, or specific inorganic salts were involved, showing the simplicity of this method. Furthermore, the as-prepared α-Fe_2O_3 porous nanospheres exhibit excellent sensing performance towards ethanol, formaldehyde, and acetic acid at a low working temperature.

Acknowledgment

This work was financially supported by the Australian Research Council (ARC) through an ARC Discovery Project (DP0559891).

References

[1] Kong J, Franklin N R, Zhou C, Chapline M G, Peng S, Cho K and Dai H 2000 *Science* **287** 622
[2] Law M, Kind H, Messer B, Kim F and Yang P D 2002 *Angew. Chem. Int. Edn* **41** 2405
[3] Wang Y L, Jiang X C and Xia Y N 2003 *J. Am. Chem. Soc.* **125** 16176
[4] Kolmakov A and Moskovits M 2004 *Annu. Rev. Mater. Res.* **34** 151
[5] Lieber C M and Wang Z L 2007 *MRS Bull.* **32** 99
[6] Chen J, Xu L, Li W and Gou X 2005 *Adv. Mater.* **17** 582
[7] Sun Z, Yuan H, Liu Z, Han B and Zhang X 2005 *Adv. Mater.* **17** 2993
[8] Hermanek M, Zboril R, Medrik I, Pechousek J and Gregor C 2007 *J. Am. Chem. Soc.* **129** 10929
[9] Cesar I, Kay A, Gonzalez Martinez J A and Grätzel M 2006 *J. Am. Chem. Soc.* **128** 4582
[10] Zhong L, Hu J, Liang H, Cao A, Song W and Wan L 2006 *Adv. Mater.* **18** 2426
[11] Wu P, Wang W, Huang Y, Shen H, Lo Y, Tsai T, Shieh D and Yeh C 2007 *Chem. Eur. J.* **13** 3878
[12] Cao M, Liu T, Gao S, Sun G, Wu X, Hu C and Wang Z L 2005 *Angew. Chem. Int. Edn* **44** 4197
[13] Wen X, Wang S, Ding Y, Wang Z L and Yang S 2005 *J. Phys. Chem.* B **109** 215
[14] Hu X, Yu J C, Gong J, Li Q and Li G 2007 *Adv. Mater.* **19** 2324
[15] Gurlo A and Riedel R 2007 *Angew. Chem. Int. Edn* **46** 3826
[16] Tiemann M 2007 *Chem. Eur. J.* **13** 8376
[17] Jiao F, Harrison A, Jumas J, Chadwick A V, Kockelmann W and Bruce P G 2006 *J. Am. Chem. Soc.* **128** 5468
[18] Liu L, Kou H, Mo W, Liu H and Wang Y 2006 *J. Phys. Chem.* B **110** 15218
[19] Bang J H and Suslick K S 2007 *J. Am. Chem. Soc.* **129** 2242
[20] Qian H, Lin G, Zhang Y, Gunawan P and Xu R 2007 *Nanotechnology* **18** 355602
[21] Jia C, Sun L, Yan Z, You L, Luo F, Han X, Pang Y, Zhang Z and Yan C 2007 *Angew. Chem. Int. Edn* **44** 4328
[22] Wu C, Yin P, Zhu X, OuYang C and Xie Y 2006 *J. Phys. Chem.* B **110** 17806
[23] Bersani D, Lottici P P and Montenero A 1999 *J. Raman Spectrosc.* **30** 355
[24] Hu X, Yu J C and Gong J 2007 *J. Phys. Chem.* C **111** 11180
[25] Binions R, Carmalt C J and Parkin I P 2007 *Meas. Sci. Technol.* **18** 190